# Additively Manufactured mm-Wave Multichip Modules With Fully Printed "Smart" Encapsulation Structures

Xuanke He, *Student Member, IEEE*, Bijan K. Tehrani, *Student Member, IEEE*, Ryan Bahr, *Student Member, IEEE*, Wenjing Su, *Member, IEEE*, and Manos M. Tentzeris, *Fellow, IEEE*

***Abstract*— This article presents the first time that an millimeter-wave (mm-wave) multichip module (MCM) with on-demand "smart" encapsulation has been fabricated utilizing additive manufacturing technologies. RF and dc interconnects were fabricated using inkjet printing, while the encapsulation was realized using 3-D printing. Inkjet-printed interconnects feature superior RF performance, better mechanical reliability, and on-demand, low-cost fabrication process. Numerous test vehicles were initially produced to evaluate these additive manufacturing technologies and compare them with traditional ribbon bonding, exhibiting a superior |S21| performance throughout the whole operation range up to 40 GHz with a peak of 3.3 dB better gain for a Ka-band low noise amplifier (LNA). A fully functioning front-end MCM was fabricated using the same inkjet-printed interconnect technology, which features smart encapsulation technology fabricated using the 3-D printing and integrated on-demand "smart" encapsulation for electromagnetic interference (EMI) mitigation. The proof-of-concept MCM demonstrates exceptional performance taking advantage of a low-cost, on-demand additive manufacturing method that requires minimal tooling and process steps, which can drastically accelerate the time to market for future 5G and Internet-of-Things applications. The methodologies presented in this article could potentially enable rapid production of high-performance, high-frequency customizable circuit packaging structures with on-demand "smart" features, such as self-diagnostics, EMI/EMC filtering, and integrated sensors.**

***Index Terms*— Additive manufacturing, frequency-selective surface (FSSs), inkjet printing, interconnects, millimeter wave (mm-wave), monolithic microwave integrated circuit (MMIC), multichip module (MCM), RF packaging, ribbon bonding, 3-D printing.**

## I. Introduction

As MORE and more wireless and mobile devices get added into the wireless spectrum, lower frequency bands are becoming increasingly cluttered and devices are constantly competing for enough bandwidth. Currently, there has been a push to move toward higher bandwidth, higher frequency communication channels for 5G and radar applications, featuring dramatically higher data rates that take advantage of the uncluttered frequency bands around 24 GHz or higher. As the devices move up in frequency and consequently move down in wavelength, components become smaller and can be more readily integrated into systems. However, shorter wavelength/higher frequency means larger path losses, requiring many small cells or repeaters for optimal communication channels. Adding multiple cells adds cost and slows down the implementation of 5G, issues effectively addressed by additive manufacturing methods, such as inkjet and 3-D printing. Additive manufacturing can dramatically speed up the implementation of 5G networks. Not only do they reduce manufacturing cost by simplifying the traditional multistep fabrication methodologies of photomasking, lithography, etching, and so on but also allowing print-on-demand capabilities and enabling the realization of a multitude of customized parts that can be assembled quickly and cheaply, reducing the development of a concept to final product from weeks to just hours [1]. The use of inkjet printing and 3-D printing to make RF components, such as passives, waveguides, transmission lines, and antennas, has been previously demonstrated and continues to grow in maturity [2]–[5], but its uses in packaging are still under investigation. However, some have heralded that additive manufacturing in electronics integration can help push "beyond Moore's" [6].

Packaging is a major component in 5G systems and is an excellent candidate for additive manufacturing. Typically, interconnects between the chips at millimeter-wave (mm-wave) frequencies utilize thermosonic ribbon or wirebonds to bridge ICs together as well as to allow communication to the host packaging substrate or printed circuit board (PCB). However, these methods can introduce a long loop length, large parasitic inductance at high frequencies, and greater discontinuities [7]. It can also lead to unintended radiation losses due to the high-arching bond wires [8]. Inkjet-printed interconnects feature a more rugged, planar and conformal structure, which offers an improved RF performance even in challenging configurations. Using higher performance inkjet-printed interconnects allows designers to create more efficient systems, integrating multiple chips into compact miniaturized

Manuscript received August 22, 2019; revised October 26, 2019; accepted November 11, 2019. Date of publication December 25, 2019; date of current version July 1, 2020. This work was supported in part by Lockheed Martin Corporation. *(Corresponding author: Xuanke He.)*

The authors are with the School of Electrical and Computer Engineering, Georgia Institute of Technology, Atlanta, GA 30332 USA (e-mail: xhe53@gatech.edu).

Color versions of one or more of the figures in this article are available online at http://ieeexplore.ieee.org.

Digital Object Identifier 10.1109/TMTT.2019.2956934

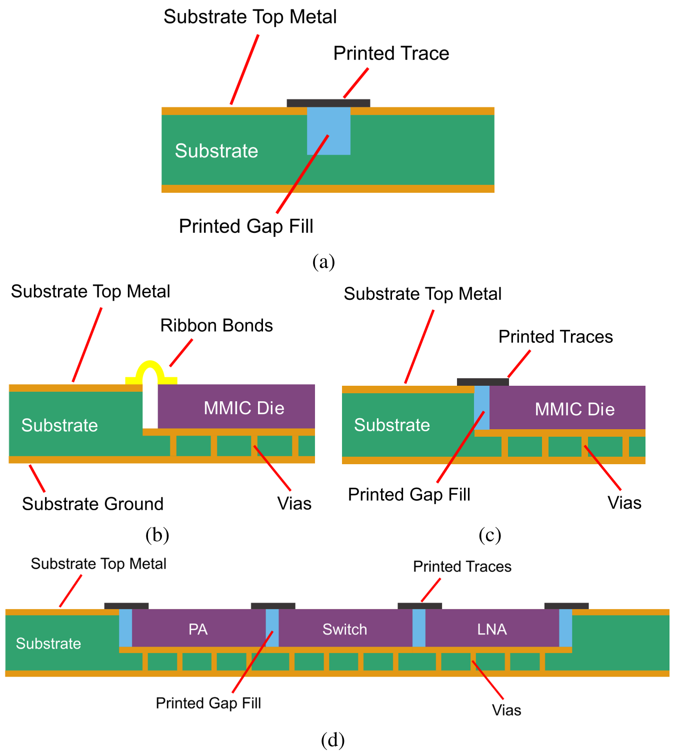


Fig. 1. Side-view schematics summary of the printed gap-filled interconnect topologies discussed in this article. (a) Printed trace interconnect over a printed gap fill to compare with a standard (continuous) microstrip transmission line. (b) and (c) Ribbon-bonded LNA MMIC comparison with an inkjet-printed LNA MMIC. (d) Fully inkjet-printed interconnected RF front-end MCM.

multilayer RF modules. Packaging mm-wave devices also typically requires encapsulation using an air cavity encapsulant to minimize dielectric loading on the chip, which is an expensive process. This can be replaced with 3-D printed encapsulation, where the air cavity is easily printed onto the modules. Additionally, multiple functionality, such as frequency-selective surfaces (FSSs), can be integrated on top for additional functionality, such as electromagnetic interference (EMI) protection. These fully printed multichip modules (MCMs) demonstrate the high level of integration and cheap manufacturing cost that is capable of using additive manufacturing.

This article begins with a demonstration of inkjet-printed interconnects where two 50-Ω microstrip transmission lines are connected using printed transmission lines to evaluate the losses compared to a regular transmission line. Additionally, Ka-band low noise amplifiers (LNAs) are interconnected using the inkjet printing technology, while another two samples are interconnected using ribbon bonds to evaluate the interconnect performance on active monolithic microwave integrated circuits (MMICs). All test vehicles are fabricated on the exact same substrate material to keep assembly characteristics consistent. The work is then extended to a real-world RF front-end module application integrating LNA, power amplifier (PA), and switch MMICs, which is fully encapsulated using 3-D printing and features an integrated FSS for EMI mitigation. The summary of the fully printed gap-filled interconnects discussed in this article is shown in a schematic form in Fig. 1, and the complete additively manufactured RF front-end MCM module is shown in Fig. 2 in the 3-D form.

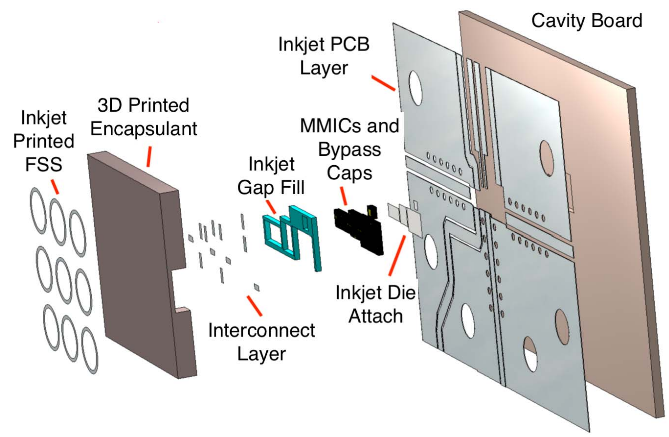


Fig. 2. Exploded view of the complete encapsulated RF front-end MCM, showing the multiple layers that were additively manufactured.

In this article, all chips were mounted in a surface-mounting fashion, meaning that the bond pads for the chip are facing upward. The alternative to this is flip-chip technology. However, flip-chip assembly yields a lower throughput from a manufacturing standpoint in addition to requiring very flat surfaces, underfilling layers, and accurate pick-and-place. Additionally, many mm-wave ICs require backside grounding that is not possible with flip chip [9]. Other works regarding packaging of mm-wave/high-frequency devices have utilized aerosol jet printing for mm-wave packaging such as [10]–[12] but only on simple passive structures. Compared to inkjet printing, aerosol jet printing offers an increased resolution but at a higher operating cost while utilizing only a few printing nozzles, compared to the thousands available on a commercial inkjet printhead, making it less suitable for large-scale production settings. Similar works, such as [13], demonstrate the inkjet-printed ramp interconnects with active devices and [14] discuss a cavity-embedded chip on a 3-D printed substrates. However, the ramped structure in [13] lacks a good grounding of the chip and mechanical stability of cavity embedding and [14] features wirebonded interconnects, for which this article that will demonstrate is an inferior interconnect technique. References [15] and [16] demonstrated a D-band MCMs' technology that is fabricated partially using 3-D printing, but the process is not entirely additive since it uses multistep masking lithography to build the 3-D structure, polymerizing and liftoff processes, and additionally does not fully demonstrate the multichip aspect of the MCM since there is only one active chip. Other works have also demonstrated 3-D printed chip encapsulations, such as [17] and [18], but the chip that was encapsulated was a dummy and lacked quantifiable results. This article presents for the first time to the authors' knowledge that such an MCM system in the mm-wave regime with this level of integration has been characterized, fabricated, and encapsulated entirely using additive manufacturing.

## II. Fabrication Methodology

Cavity-embedding MMICs are a common practice in the fabrication of packaged microwave components.

When MMICs are placed within a cavity, there is a gap between the chip and the outside metal connections, which is typically bridged with bond wires or ribbons, as shown in Fig. 1(b). Bond wires are nonplanar and typically feature an arching shape, which effectively increases the length of the wire. Increasing the wire length would, in turn, increase the mismatch due to a larger inductance and a larger discontinuity between the chip pads and the transmission lines. To reduce the length-induced wire inductance, inkjet-printed interconnects are proposed as an alternative; a novel inkjet printing approach presented in this article addresses the need for an accurate filling of the gap between the MMIC and the substrate with a dielectric in a smooth fashion despite its very steep transitions.

The materials required for the printed interconnect prototypes were inkjet printed using a Dimatix-2800 series inkjet printer. An SU8 photoresist ink was inkjet printed as the dielectric material, and the metallization was accomplished using Suntronic EMD5730 silver nanoparticle (SNP) ink from Sun Chemical. SU8 has a dielectric constant of 2.85 and a loss tangent of 0.04 at above 20 GHz [19] and is formulated according to [20] to have a viscosity of 13 cP, making it suitable for inkjet printing. The Suntronic EMD5730 has a volume resistivity of 5–30 $\mu\Omega \cdot$ cm according to the manufacturer's datasheet. The LNA used for the characterization of the interconnects is the Analog Devices ALH369 Ka-band amplifier that was embedded in a 10 mil (0.25 mm) thick MEG-6 substrate, with a dielectric constant of 3.6 and a loss tangent of 0.005, from Matrix Materials. To create an evaluation vehicle for this article, an evaluation circuit board was milled out of the MEG-6 substrate. For the application demonstrator, the front-end MCM, the same ALH369 LNA was utilized in conjunction with Qorvo TGA 4036 PA and Qorvo TGS 4302 SPDT switch on 12-mil Rogers 4003C shown in Fig. 1(d). TGS4302 acts as the switch in the transceiver, selecting between the receiver and the transmitter MMICs, with a shared output port. The circuit is fully printed using inkjet printing. The encapsulation for the front-end MCM is 3-D printed using the FormLabs Form 2 printer using high-temperature resin (FLHTAM02 V2), which can withstand the sintering temperature of the printed SNPs at 150 °C without warping.

For the printed interconnects, a major challenge is to choose the material and the correct printing process to achieve a smooth gap fill. Solvent-based dielectric inks exhibit volume loss during curing, meaning that the height of the dielectric is difficult to predict, which commonly leads to unconnected interconnects. SU8 was used as the gap-filling dielectric material since it can be inkjet printed at high volumes with a relatively low volume loss. A rigorous evaluation of the SU8 gap fill was performed to observe the correct amount of SU8 to print to get a smooth transition. It was observed that eight layers of SU8 were needed at 15-$\mu$m drop spacing, equivalent to 1693 drops/in with 10-pL volume size per ink droplet, to fill a gap that is 100 $\mu$m deep. Fig. 3 shows the profilometer scan of the cavity before and after gap filling, and from this, it is observed that the SU8 formed a smooth transition from the substrate to the die edge. The SU8 was printed at a 60 °C stage temperature, and UV crosslinked at 500 mJ/cm$^2$ and hardbaked at 155 °C for 30 min. Finally, three layers, which correspond to around 5-$\mu$m metal thickness, of SNP ink, at 20-$\mu$m drop spacing, were printed as interconnects for pad-to-pad or pad-to-board connections. The SNP ink was sintered at 150 °C for 30 min. The proof-of-concept front-end MCM is interconnected in an identical fashion, except with the board-level circuitry also additively printed. The encapsulant is 3-D printed using FormLabs Form 2 High Temperature material and was adhered around the chip on the board using inkjet-printed SU8 epoxy. The additional FSS features printed on the top of the encapsulant were inkjet printed using the identical SNP printing techniques described previously.

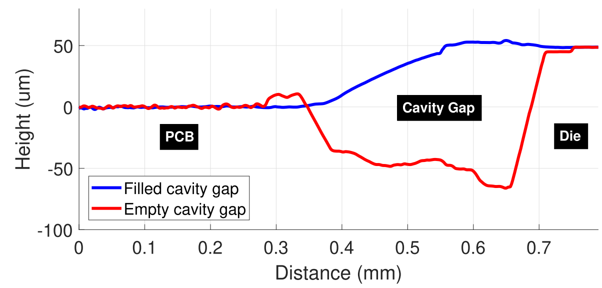


Fig. 3. Profilometer scan of the transition area from evaluation board to chip. The red line shows the profile pregap filling, and the blue solid line is postgap filling. The postgap fill shows a smooth transition from the PCB to die edge.

## III. Measurements

Three different test vehicles were fabricated in this article to evaluate this novel packaging technique. Initially, a completely passive transmission line structure was fabricated with a 400-$\mu$m-wide, 100-$\mu$m-deep gap separating the two transmission lines. Another continuous (no gap) transmission line was also fabricated on the same substrate with the same dimensions was used as a benchmarking reference for the printed interconnects to compare the losses between the two. Second, the active ALH369 LNA was connected using the same inkjet-printed technique, with 2 fabricated to evaluate the consistency. Using the same evaluation board, two ribbon-bonded LNA samples were fabricated and used as a test benchmark against the inkjet-printed samples. Finally, an entire MCM utilizing three distinct MMICs was fabricated and encapsulated.

### *A. Transmission Line*

As an initial technology demonstrator, interfacing two passive structures was seen as the most logical first step. Two 50-$\Omega$ transmission lines on the MEG6 substrate were fabricated with a separation gap distance of 400 $\mu$m. This distance was chosen for a few reasons. First, it considers milling accuracy, and second, it gives spacing for the ribbon bonder to make a good bond due to the size of the ultrasonic head. A 100-$\mu$m-deep gap was then milled into the substrate, creating a cavity. An equivalent circuit for the proposed inkjet-printed interconnect is shown in Fig. 4 based on models found in the literature. The gap-filling process is shown in Fig. 5,

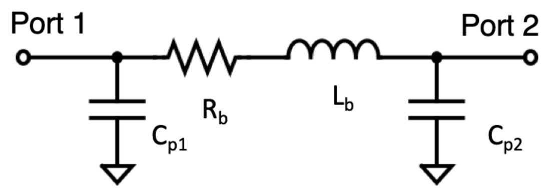


Fig. 4. Equivalent circuit diagram for the inkjet-printed interconnect based on [21] and [22]. $C_{p1}$ = $C_{p2}$ = 55 fF, $L_b$= 0.27 nH, and $R_b$ = 0.9 Ω.

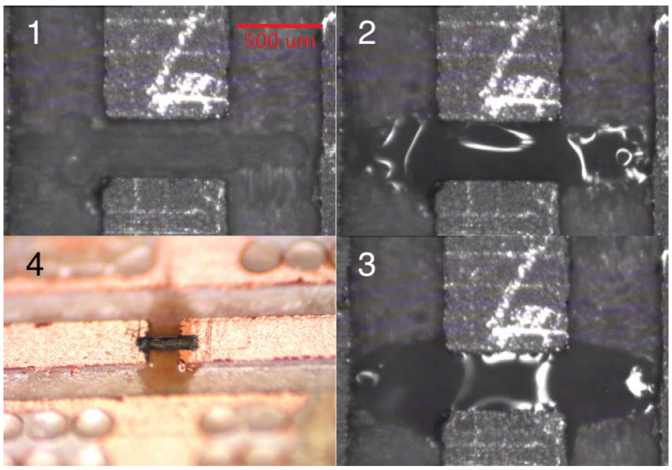


Fig. 5. Fabrication steps of the inkjet-printed "gap-filled" interconnects (clockwise). 1: empty cavity between two transmission lines. 2: Su8 gap filling showing an underfilled gap. 3: perfectly filled gap. 4: SNP interconnect printed on top of the SU8.

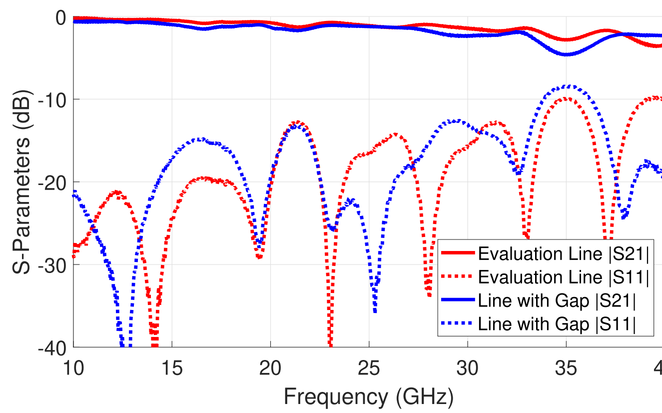


Fig. 6. $|S11|$ and $|S21|$ comparison between a regular thru transmission line and interconnected transmission line structures using inkjet printing techniques.

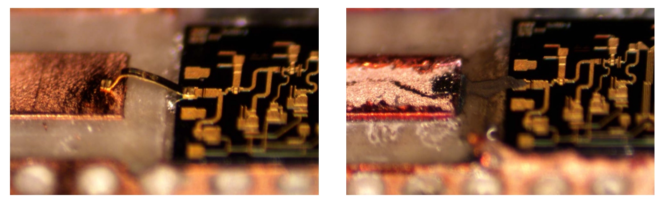

(a) (b)

Fig. 7. Proof-of-concept prototype images of the cavity-embedded LNA MMIC with (a) ribbon bonds and (b) printed interconnects at the RF input.

and it is visually clear that the inkjet-printed dielectric SU8 material completely filled the cavity creating a smooth transition between the two transmission lines. Following UV cure and postbaking, a small interconnect that was 75 $\mu$m in width was printed to bridge the two transmission lines. Southwest Microwave end-launch connectors were attached to the two ends of the transmission lines in order to facilitate VNA measurements. Measurements that were taken of the return loss and insertion loss of the printed interconnect were plotted in comparison to a continuous thru transmission. The data in Fig. 6 show an approximate 0.5-dB nominal degradation from a regular transmission line |S21|, with an exception at 35 GHz, where the printed interconnect experiences a slight resonance with the insertion loss dipping −2.5 dB. This is experimentally found to be due to the increased inductance, which causes a resonance in the printed interconnect versus a regular transmission line. This resonance can be reduced by printing a thicker trace, but the trace thickness is limited by the chip pad dimensions discussed later in this article.

## B. Active Devices

To evaluate the performance of the inkjet-printed interconnect technology in real-world applications, active devices underwent the same inkjet-printed gap-filling interconnect fabrication process. Traditionally, MMIC devices require ribbon bonding for the RF interconnects, so it is necessary to offer a comparison between the traditional and the new technique. Fig. 7 shows the perspective images of the bonded and printed transitions with the proof-of-concept LNA ICs. In order to evaluate this effectiveness, LNA evaluation boards were fabricated using an identical milling and chip placement process. Two samples utilizing each technique were fabricated to ensure reliability and consistency. The gaps between the chip edge and the transmission lines were also kept at the same spacing as in the previous transmission-line characterization, 400 $\mu$m. This distance was chosen for two reasons. First, it allows extra spacing to prevent die-attach spreading, which can lead to short circuit of the transmission line; second, it gives spacing for the ribbon bonder to make a good connection due to the size of the ultrasonic head. Optimally, shorter interconnects are better, but the ribbon bonds in this article were kept at the lowest possible length due to these factors and are shorter in length than in other RF bonds found in other literature [23]–[25]. The ribbon bond interconnects had an average length of 550 $\mu$m, a width of 75 $\mu$m, and an average height of 132 $\mu$m. The length of the bond wire increased due to the increase in bond height and because of the additional wedge length needed to create a solid connection.

The S-parameters for the printed and bonded transitions are shown in Fig. 8. Return loss measurements show a clear improvement in matching for the inkjet-printed transitions across the whole measured band due to the reduced interconnect length and profile height. Gain measurements show relatively similar trends for both printed and bonded transitions.

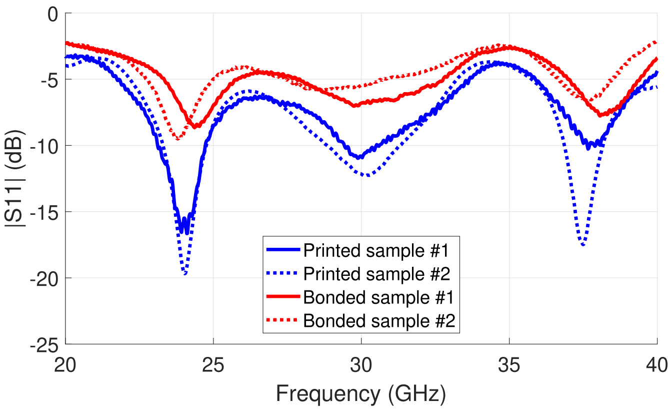


Fig. 8. Measured S-parameters for cavity-embedded LNA MMIC with printed transitions and ribbon bonds demonstrating an improvement in $|S11|$ performance due to the shorter bond length.

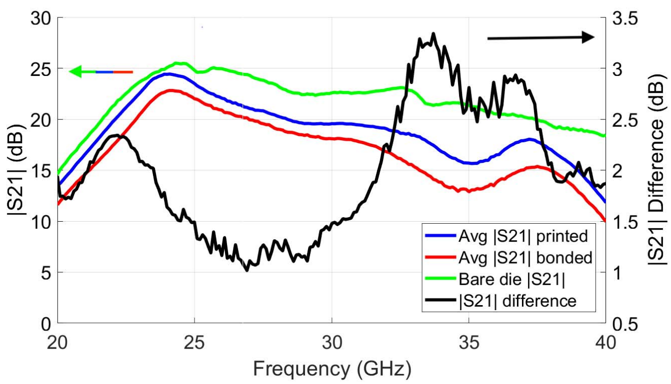


Fig. 9. Left axis: average insertion loss for printed and bonded samples. Right axis: difference in insertion loss between the printed and bonded samples (printed minus bonded). The bare die (without interconnects or evaluation board) measurement is shown in green as a reference.

In an effort to better understand the effects of the proposed interconnects on amplifier gain, the |S21| measurements of the two printed and two bonded interconnect devices are averaged accordingly and subtracted from one another to identify the difference in gain. Fig. 9 shows the average gain versus frequency of the LNA with printed and bonded transitions (left axis). The average |S21| measurements for bonded transitions are subtracted from the average |S21| of the printed transitions, yielding a plot of |S21| difference presented in Fig. 9 (right axis). From the measurements, it is clear that due to the decreased interconnect length and inductance, better matching was achieved, leading to a better insertion loss/gain performance. The average increase in the gain is at least 1 dB and with a peak of 3.3-dB improvement over the whole frequency range of 20–40 GHz. The improvement is especially noticeable in 30 GHz and above where the decreased inductance in the inkjet-printed interconnect translates to a weaker resonance.

### *C. Front-End MCM*

The front-end MCM consisting of three active MMICs along with a smart encapsulation is the final proof-of-concept demonstrator of this article. With the characterization of the inkjet-printed interconnects complete, fully functioning systems can utilize the inkjet printing technology for interconnects. The ALH369 LNA was used as the receiver IC, the TGA4036 was used as the transmitter IC, and TGS4302 was used as the switching module between the TX/RX and the

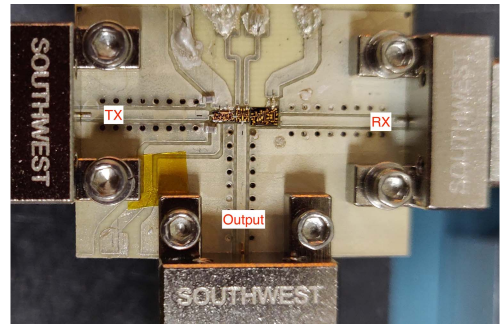


(a)

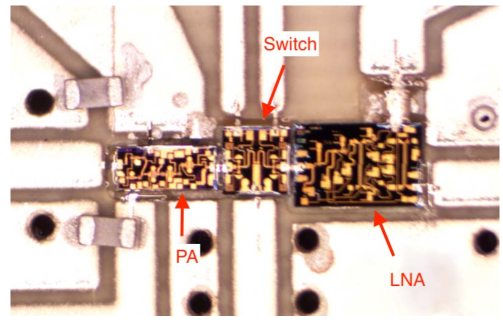


(b)

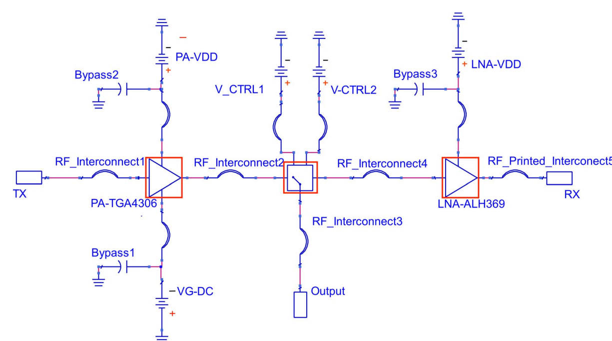


(c)

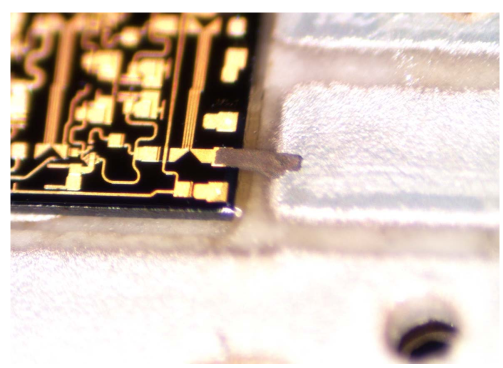

(d)

Fig. 10. Nonencapsulated mm-wave front-end MCM fabricated using inkjet printing. (a) Full system interfaced with southwest end-launch connectors. (b) zoomed-in. (c) Schematic of the front-end MCM. (d) One of the inkjet-printed RF interconnects on the output of the LNA.

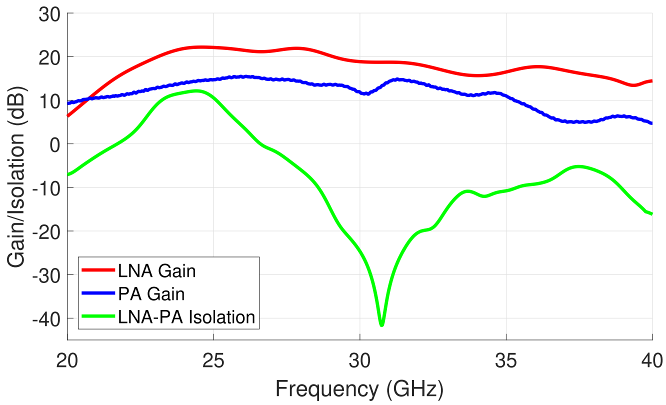


Fig. 11. S-parameters of the front-end module. Both LNA and PA |S21| are measured, along with isolation between the two when LNA and PA are both turned on. The resonance seen in the isolation is an inherent characteristic of the switch IC.

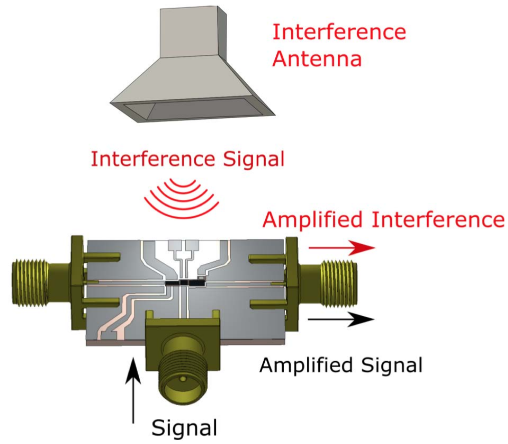


Fig. 12. Measurement setup of EMI of the front-end MCM utilizing an 18 dBi horn antenna as a potential interference source. In the setup, the horn antenna was placed 40 cm away from the module and the amplified interference signal was measured.

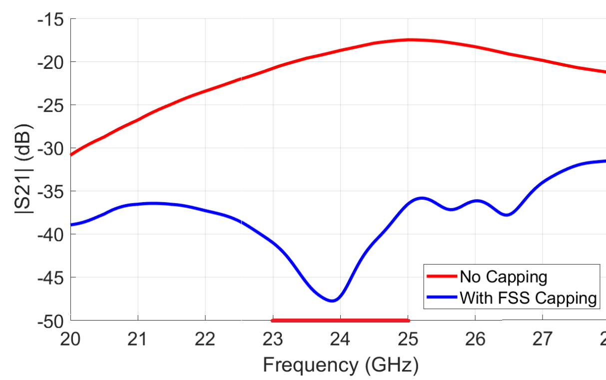


Fig. 13. Simulation of the FSS EMI measurement setup, showing a decrease in LNA receiver interference within the 24-GHz 5G bands, which is due to the $3 \times 3$ FSS. Port 1 would be the horn antenna port, and port 2 is output amplifier port.

shared output port, allowing for time-domain duplexing in the same module. All the packaging is done in a fully additive fashion. Instead of the copper circuit board interface, the entire circuit board conductor layer was inkjet printed on Rogers 4003C instead of MEG 6 due to the better adhesion SNP on the Rogers substrate. This enhances the speed of production and reduces the tooling required as a major portion of the fabrication process is done on a single inkjet printer. The system is shown in Fig. 10. The module's S-parameter performance is plotted in Fig. 11, demonstrating the performance of both TX and RX chains and the isolation between the TX and RX paths. From Fig. 11, both the LNA and PA turn on and provided gain, which is nominally around 3.5–4 dB below the bare die measurements. This considers the losses of the switch MMIC and additional chip-to-chip (PA to switch and switch to LNA) interconnects and the transmission line losses and Southwest connectors, which is in line with the expected losses from this system.

Additionally, the devices were encapsulated for environmental shielding purposes with a cavity to reduce dielectric loading on the front-end MCM. The nature of the additive manufacturing method allows for a straightforward incorporation of "smart" features on the encapsulation structure. A circular ring FSS was designed at around 24 GHz in order to block out interference in this band of interest. The encapsulation has an air cavity that is 1 mm in height with the thickness of the encapsulant being 0.2 mm, making the total encapsulant height 1.2 mm. The FSS is then printed on top of this 1.2-mm encapsulation structure. Simulation of the FSS was conducted using the Floquet port simulation method in CST Microwave Studio and following design guidelines outlined in [26] and [27], and the circular unit cells were kept at around one wavelength at 24 GHz. Due to the size constraints, only a $3 \times 3$ FSS was utilized. From the S-parameter data previously shown, the front-end MCM can cover the 5G mm-wave frequency bands, and thus, it is imperative that the module's sensitivity is not degraded by the adjacent bands or other mm-wave frequency sources during operation when using a particular frequency.

In order to evaluate RX EMI susceptibility, simulations and measurements were set up to evaluate a potential interferer's effect on the module, as shown in Fig. 12. In the simulation, the on-package $3 \times 3$ FSS was placed between a CST model of the horn antenna, placed 40 cm away from the module, and a waveguide port. The target frequencies for the FSS to block are a 2-GHz bandwidth around 24 GHz, which covers a good portion of the 24-GHz 5G band and other point-to-point communication standards. Due to the 3-D electromagnetic (EM) model of the chip that was not readily available, a waveguide port was used instead for evaluation purposes to simulate the interference received by the IC. A rough estimate of the interference signal attenuation using the free space path loss equation at 40 cm in addition to the gain of the LNA at 24 GHz (23 dB) results in a combined interference signal attenuation of only around 11 dB, which is approximately what is shown in the simulations in Fig. 13. The simulation results demonstrate a clear filter response at around 24 GHz due to the $3 \times 3$ FSS capping compared to the baseline, with no FSS capping in between the two waveports. The fabricated 3-D printed encapsulant on top of the MCM is shown in Fig. 14.

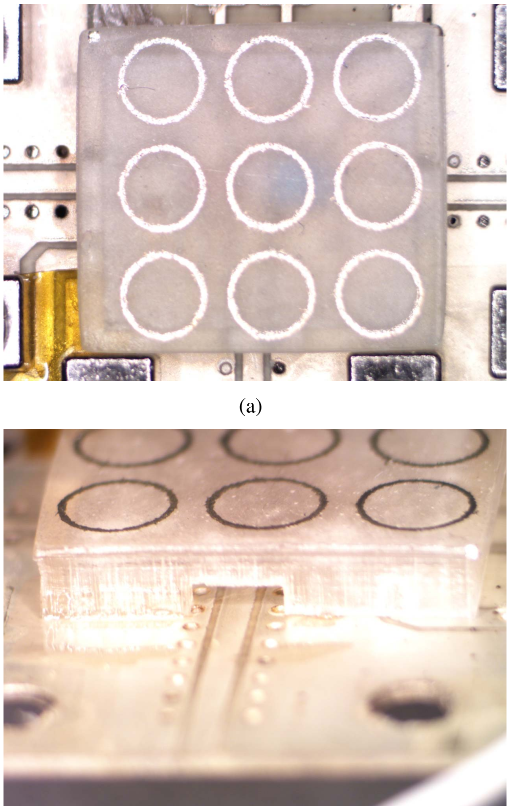

(a)

(b)

Fig. 14. (a) 24-GHz FSS inkjet printed on top of the 3-D printed encapsulation. (b) Perspective image showing cavity encapsulation of the front-end MCM.

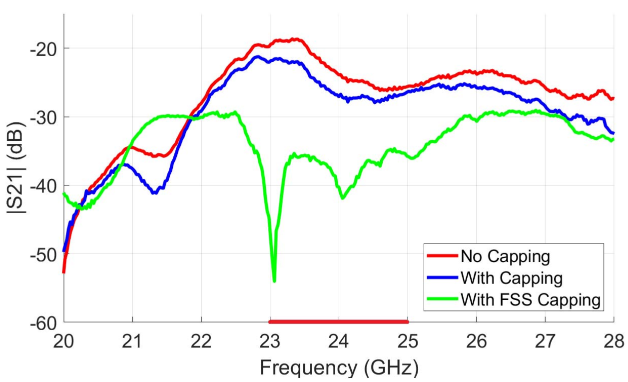


Fig. 15. EMI measurements pre- and post-encapsulation with FSS, demonstrating a large increase in EMI isolation from 23- to 25-GHz range. Differences in measurement and simulation occur due to the 3-D EM models of the chip not being readily available.

Fig. 15 shows the data collected from the measurement setup, and pre- and post-encapsulation. Prior to the encapsulation, the bare die MCM observed poor EMI shielding, as the LNA amplified the incoming interference signal, with only about −20-dB signal transmission from the interference antenna to the output of the LNA in this test setup. Following the printing of the FSS on top of the encapsulant, an extra >18 dB of isolation was observed at 24 GHz, a large improvement from the bare die measurement, with no effect on the |S21| performance of the MCM. This enhances the capabilities of the module providing features that enhance EMI shielding and helps to reduce desense, degredation of sensitivity, and lays the groundwork for more advanced "smart" features to be incorporated into the packaging, such as sensors or antennas.

## IV. Conclusion

In this article, the fundamental additive manufacturing technology of inkjet-printed interconnects is characterized for passive devices and active MMICs, exhibiting minimal losses across the majority of the 5G mm-wave frequency bands. This article also demonstrates for the first time a low-cost additive manufacturing approach for fully printed packaging of mm-wave MCM systems, which incorporates "smart" encapsulation in the form of a frequency-selective EMI shield. Additional research is focusing on further integration of MMICs and other components. This includes incorporating additional front-end elements, such as mixers and oscillator ICs and printing on-package antennas, to create fully integrated front-end MCM devices for 5G and Internet-of-Things (IoT) applications. Additionally, this technique of inkjet-printed interconnects increases the reliability of devices because it removes free-standing bond wires and provides a mechanical stress buffer for the cavity-embedded MMICs. However, additional quantitative work needs to be done to evaluate the reliability of this technique for use in high-reliability aerospace or military applications. With low-cost and highly scalable additive manufacturing, wireless circuits and electronics can be rapidly prototyped and deployed into different environments. This article paves the way for future work regarding highly customizable, heterogeneously integrated high-performance mm-wave systems that are cheap to manufacture, quick to implement to production, and require simple and minimal tooling.

## Acknowledgment

The authors would like to thank D. Fanning and G. Romas of Lockheed Martin for their help in the inkjet printing interconnect characterization efforts.

## References

[1] E. MacDonald *et al.*, "3D printing for the rapid prototyping of structural electronics," *IEEE Access*, vol. 2, pp. 234–242, 2014.

[2] B. S. Cook, J. R. Cooper, and M. M. Tentzeris, "Multi-layer RF capacitors on flexible substrates utilizing inkjet printed dielectric polymers," *IEEE Microw. Wireless Compon. Lett.*, vol. 23, no. 7, pp. 353–355, Jul. 2013.

[3] G. P. Le Sage, "3D printed waveguide slot array antennas," *IEEE Access*, vol. 4, pp. 1258–1265, 2016.

[4] C. Kim *et al.*, "3D printed electronics with high performance, multi-layered electrical interconnect," *IEEE Access*, vol. 5, pp. 25286–25294, 2017.

[5] B. Zhang and H. Zirath, "A metallic 3-D printed e-band radio front end," *IEEE Microw. Wireless Compon. Lett.*, vol. 26, no. 5, pp. 331–333, May 2016.

[6] J. Veres *et al.*, "Additive manufacturing for electronics 'Beyond Moore,'" in *IEDM Tech. Dig.*, Dec. 2016, pp. 25.6.1–25.6.3.

[7] T. Krems, W. Haydl, H. Massler, and J. Rudiger, "Millimeter-wave performance of chip interconnections using wire bonding and flip chip," in *IEEE MTT-S Int. Microw. Symp. Dig.*, vol. 1, Jun. 1996, pp. 247–250.

[8] I. Ndip *et al.*, "Modelling the shape, length and radiation characteristics of bond wire antennas," *IET Microw., Antennas Propag.*, vol. 6, no. 10, pp. 1187–1194, Jul. 2012.

[9] G. Pascariu, P. Cronin, and D. Crowley, "Next generation electronics packaging utilizing flip chip technology," in *Proc. IEEE/CPMT/SEMI 28th Int. Electron. Manuf. Technol. Symp. (IEMT)*, Jul. 2003, pp. 423–426.

[10] M. T. Craton, J. D. Albrecht, P. Chahal, and J. Papapolymerou, "A chip-first approach to millimeter-wave circuit packaging," *IEEE Microw. Wireless Compon. Lett.*, pp. 1–3, 2019.

[11] C. Armiento, S. Trulli, A. Akyurtlu, E. Harper, M. Haghzadeh, and C. Laighton, "Printed electronics and additive packaging for microwave applications," in *Proc. Int. Conf. Electron. Packag. (ICEP)*, Apr. 2017, pp. 1–2.

[12] F. X. Röhrl, J. Jakob, W. Bogner, R. Weigel, and S. Zorn, "Bare die connections via aerosol jet technology for millimeter wave applications," in *Proc. 48th Eur. Microw. Conf. (EuMC)*, Sep. 2018, pp. 1033–1036.

[13] B. K. Tehrani and M. M. Tentzeris, "Fully inkjet-printed ramp interconnects for wireless Ka-band MMIC devices and multi-chip module packaging," in *Proc. 48th Eur. Microw. Conf. (EuMC)*, Sep. 2018, pp. 1037–1040.

[14] S. Pavlidis, B. Wright, and J. Papapolymerou, "3-D printed substrates for MMIC packaging," in *Proc. IEEE Radio Wireless Symp. (RWS)*, Jan. 2017, pp. 79–82.

[15] T. Merkle, R. Götzen, J. Y. Choi, and S. Koch, "Polymer multichip module process using 3-D printing technologies for D-band applications," *IEEE Trans. Microw. Theory Techn.*, vol. 63, no. 2, pp. 481–493, Feb. 2015.

[16] T. Merkle and R. Götzen, "Millimeter-wave surface mount technology for 3-D printed polymer multichip modules," *IEEE Trans. Compon., Packag., Manuf. Technol.*, vol. 5, no. 2, pp. 201–206, Feb. 2015.

[17] B. K. Tehrani, R. A. Bahr, W. Su, B. S. Cook, and M. M. Tentzeris, "E-band characterization of 3D-printed dielectrics for fully-printed millimeter-wave wireless system packaging," in *IEEE MTT-S Int. Microw. Symp. Dig.*, Jun. 2017, pp. 1756–1759.

[18] B. K. Tehrani, B. S. Cook, and M. M. Tentzeris, "Inkjet-printed 3D interconnects for millimeter-wave system-on-package solutions," in *IEEE MTT-S Int. Microw. Symp. Dig.*, May 2016, pp. 1–4.

[19] A. Ghannam, C. Viallon, D. Bourrier, and T. Parra, "Dielectric microwave characterization of the SU-8 thick resin used in an above ic process," in *Proc. Eur. Microw. Conf. (EuMC)*, Sep./Oct. 2009, pp. 1041–1044.

[20] B. K. Tehrani, C. Mariotti, B. S. Cook, L. Roselli, and M. M. Tentzeris, "Development, characterization, and processing of thin and thick inkjet-printed dielectric films," *Organic Electron.*, vol. 29, pp. 135–141, Feb. 2016. [Online]. Available: http://www.sciencedirect.com/science/article/pii/S1566119915302032

[21] D. Jahn, R. Reuter, Y. Yin, and J. Feige, "Characterization and modeling of wire bond interconnects up to 100 GHz," in *Proc. IEEE Compound Semiconductor Integr. Circuit Symp.*, Nov. 2006, pp. 111–114.

[22] I. Ndip, A. Ö, H. Reichl, K. D. Lang, and H. Henke, "Analytical models for calculating the inductances of bond wires in dependence on their shapes, bonding parameters, and materials," *IEEE Trans. Electromagn. Compat.*, vol. 57, no. 2, pp. 241–249, Apr. 2015.

[23] J. Lim, D. Kwon, J. S. Rieh, S. W. Kim, and S. W. Hwang, "RF characterization and modeling of various wire bond transitions," *IEEE Trans. Adv. Packag.*, vol. 28, no. 4, pp. 772–778, Nov. 2005.

[24] A. C. W. Lu *et al.*, "Modeling and characterization of wire bonding for RF applications," in *Proc. 52nd Electron. Compon. Technol. Conf.*, May 2002, pp. 905–909.

[25] A. Sutono, N. G. Cafaro, J. Laskar, and M. M. Tentzeris, "Experimental modeling, repeatability investigation and optimization of microwave bond wire interconnects," *IEEE Trans. Adv. Packag.*, vol. 24, no. 4, pp. 595–603, Nov. 2001.

[26] J. Huang and S. W. Lee, "Tri-band frequency selective surface with circular ring elements," in *Antennas Propag. Soc. Symp. Dig.*, vol. 1, Jun. 1991, pp. 204–207.

[27] A. R. Varkani, Z. H. Firouzeh, and A. Z. Nezhad, "Equivalent circuit model for array of circular loop FSS structures at oblique angles of incidence," *IET Microw., Antennas Propag.*, vol. 12, no. 5, pp. 749–755, Apr. 2018.


**Xuanke (Tony) He** (S'13) received the B.S. degree (Hons.) in electrical engineering from the Georgia Institute of Technology, Atlanta, GA, USA, in 2016, where he is currently pursuing the Ph.D. degree in electrical engineering at the ATHENA Research Lab.

His research focuses on using additive manufacturing to enable low-cost scalable 5G and mm-wave electronics, packaging, and antennas for applications in wireless communications, sensing, and energy harvesting. He is currently focusing on developing novel ways of utilizing additive manufacturing to further integrate microwave components into useful and cost-/space-saving devices.

**Bijan K. Tehrani** (S'13) received the B.S. and M.S. degrees in electrical engineering from the Georgia Institute of Technology, Atlanta, GA, USA, in 2013 and 2015, respectively, where he is currently pursuing the Ph.D. degree in electrical and computer engineering under the supervision of Prof. M. Tentzeris at the ATHENA Research Lab.

His research interests include the development of advanced multilayer inkjet and 3-D printing fabrication processes for the realization of additive, postprocessed millimeter-wave antenna integration for system-on-chip and system-in-package solutions.

**Ryan Bahr** (S'11) received the B.S. degree *(summa cum laude)* in RF engineering and the M.S. degree in electromagnetics with a minor in computer science from the Georgia Institute of Technology, Atlanta, GA, USA, in 2013 and 2015, respectively.

He is currently a Research Assistant with the ATHENA Research Lab, Georgia Institute of Technology, where he focuses on the development of 3-D electromagnetic designs utilizing additive manufacturing. He designs complex electromagnetic structures with additive manufacturing, including technologies such as fused deposition modeling, stereolithography, and inkjet printing. His past work has demonstrated mathematically inspired structures, inkjet printing of flexible electronics, and the utilization of additive manufacturing for RF packaging and mm-Wave electronics. More recently, he has focused on the design of gradient index structures and novel materials for low-loss, high-resolution additive manufacturing.

Mr. Bahr received the Best Student Poster Award at Gomac Tech 2016 for additively manufactured flexible and origami-reconfigurable RF sensors.

**Wenjing Su** (S'14–M'19) received the B.S. degree in electrical engineering from the Beijing Institute of Technology, Beijing, China, in 2013, and the Ph.D. degree in electrical and computer engineering from the Georgia Institute of Technology, Atlanta, GA, USA, in 2018.

In fall 2013, she joined the ATHENA Research Lab, Georgia Institute of Technology, led by Dr. M. M. Tentzeris. She is currently working at Google, Mountain View, CA, USA. Her research interfaces advance novel fabrication technique (e.g., inkjet printing and 3-D printing), special mechanical structures (e.g., microfluidics and origami), and microwave components/antennas to solve problems in smart health, wearable electronics in the Internet-of-Things (IoT) applications. She has authored over 37 articles in refereed journals and conference proceedings. She holds four patents/patent applications. Her research interests include wearable antennas, flexible electronics, applied electromagnetics, additively manufactured electronics, wireless sensing, machine-learning-aid sensing, green electronics, RFID, and reconfigurable antennas.

**Manos M. Tentzeris** (S'89–M'92–SM'03–F'10) received the Diploma degree *(magna cum laude)* in electrical and computer engineering from the National Technical University of Athens, Athens, Greece, and the M.S. and Ph.D. degrees in electrical engineering and computer science from the University of Michigan, Ann Arbor, MI, USA.

He was a Visiting Professor with the Technical University of Munich, Munich, Germany, in 2002, GTRI-Ireland, Athlone, Ireland, in 2009, and LAAS-CNRS, Toulouse, France, in 2010. He is currently a Ken Byers Professor of exible electronics with the School of Electrical and Computer Engineering, Georgia Institute of Technology, Atlanta, GA, USA, where he heads the ATHENA Research Group (20 researchers). He has served as the Head of the GTECE Electromagnetics Technical Interest Group, the Georgia Electronic Design Center Associate Director of RFID/Sensors research, the Georgia Institute of Technology NSF-Packaging Research Center Associate Director of RF Research, and the RF Alliance Leader. He has helped in developing academic programs in 3-D/inkjet-printed RF electronics and modules, exible electronics, origami and morphing electromagnetics, highly integrated/multilayer packaging for RF and wireless applications using ceramic and organic exible materials, paper-based RFID's and sensors, wireless sensors and biosensors, wearable electronics, "Green" electronics, energy harvesting and wireless power transfer, nanotechnology applications in RF, microwave MEMs, and SOP-integrated (UWB, multiband, mmW, and conformal) antennas. He has authored more than 650 articles in refereed journals and conference proceedings, five books, and 25 book chapters.

Dr. Tentzeris is also a member of the URSI-Commission D, the MTT-15 Committee, and the Technical Chamber of Greece, an Associate Member of European Microwave Association (EuMA), and a Fellow of the Electromagnetic Academy. He was a recipient/corecipient of the 2019 Humboldt Research Prize, the 2017 Georgia Institute of Technology Outstanding Achievement in Research Program Development Award, the 2016 Bell Labs Award Competition Third Prize, the 2015 IET Microwaves, Antennas, and Propagation Premium Award, the 2014 Georgia Institute of Technology ECE Distinguished Faculty Achievement Award, the 2014 IEEE RFID-TA Best Student Paper Award, the 2013 IET Microwaves, Antennas and Propagation Premium Award, the 2012 FiDiPro Award in Finland, the iCMG Architecture Award of Excellence, the 2010 IEEE Antennas and Propagation Society Piergiorgio L. E. Uslenghi Letters Prize Paper Award, the 2011 International Workshop on Structural Health Monitoring Best Student Paper Award, the 2010 Georgia Institute of Technology Senior Faculty Outstanding Undergraduate Research Mentor Award, the 2009 IEEE TRANSACTIONS ON COMPONENTS AND PACKAGING TECHNOLOGIES Best Paper Award, the 2009 E. T. S. Walton Award from the Irish Science Foundation, the 2007 IEEE AP-S Symposium Best Student Paper Award, the 2007 IEEE MTT-S IMS Third Best Student Paper Award, the 2007 ISAP 2007 Poster Presentation Award, the 2006 IEEE MTT-S Outstanding Young Engineer Award, the 2006 Asia–Pacic Microwave Conference Award, the 2004 IEEE TRANSACTIONS ON ADVANCED PACKAGING Commendable Paper Award, the 2003 NASA Godfrey "Art" Anzic Collaborative Distinguished Publication Award, the 2003 IBC International Educator of the Year Award, the 2003 IEEE CPMT Outstanding Young Engineer Award, the 2002 International Conference on Microwave and Millimeter-Wave Technology Best Paper Award (Beijing, China), the 2002 Georgia Institute of Technology–ECE Outstanding Junior Faculty Award, the 2001 ACES Conference Best Paper Award, the 2000 NSF CAREER Award, and the 1997 Best Paper Award of the International Hybrid Microelectronics and Packaging Society. He was the TPC Chair of the IEEE MTT-S IMS 2008 Symposium and the Chair of the 2005 IEEE CEM-TD Workshop. He is also the Vice-Chair of the RF Technical Committee (TC16) of the IEEE CPMT Society. He is also the Founder and the Chair of the RFID Technical Committee (TC24) of the IEEE MTT-S and the Secretary/Treasurer of the IEEE C-RFID. He is also an Associate Editor of the IEEE TRANSACTIONS ON MICROWAVE THEORY AND TECHNIQUES, the IEEE TRANSACTIONS ON ADVANCED PACKAGING, and the *International Journal of Antennas and Propagation*. He has given more than 100 invited talks to various universities and companies all over the world. He has served as one of the IEEE MTT-S Distinguished Microwave Lecturers from 2010 to 2012. He is one of the IEEE CRFID Distinguished Lecturers.